Supporting information：

Ti_4O_7-Coating Create a Highly Stable Zn Anode for Aqueous Zinc-ion Batteries

Mengjuan Chen[a,b], Yimeng Cui[a,b], Wenfeng Liu[b,c], Zhenpu Shi[a,b], Hongyu Dong[a,b], Hongyun Yue[a,b], Zhaoxia Cao[a, b], Zhansheng Lu,[c] Shuting Yang[a,b,c]*, Yanhong Yin[a,b]*

[a]School of Chemistry and Chemical Engineering, Henan Normal University, Xinxiang Henan 453007, China

[b]National & Local Engineering Laboratory for Motive Power and Key Materials, Xinxiang 453007, China

[c]School of Physics, Henan Normal University Xinxiang, 453007, China

Material

$KMnO_4$ ((AR 99.5%, Chengdu Colon Chemical Co., LTD) $MnSO_4$ H_2O (AR 99.95%, Aladdin), $ZnSO_4$ $7H_2O$ (AR Aladdin), Superconducting carbon (SP, Henan lithium power supply Co., LTD), polyvinylidene fluoride (PVDF, Henan lithium power supply Co., LTD), N-methylpyrrolidone solvent (NMP, Henan lithium power supply Co., LTD), Zn foil (purity 99.95%, 100 μm, Dongguan Kelu De experimental equipment Technology Co., LTD), glass fiber (GF/D Whatman), Ti_4O_7 (Qinghe County superenergy alloy material Co., Ltd.) Nanofibrillated Cellulose solution (NFC, Solid content 4.5±0.5%, Zhongshan nano fiber new material Co., LTD)

Experimental Section

Preparation of MnO_2 cathode. 0.1 M $KMnO_4$ and 0.7 M $MnSO_4$ were dissolved respectively in deionized water and stirred to get a uniform clear solution. Then mixing the upper two solutions and stirring at room temperature for 0.5 h before poured it into a reaction kettle and reacted at 100 ℃ for 10h. The obtained MnO_2 was washed with deionized water and ethanol for several times, and dried in a vacuum oven at 80 ℃. The prepared manganese dioxide powder, SP, and PVDF binder were mixed with NMP to form a homogeneous slurry, which was cast onto a 100 μm zinc foil by doctor blading. After drying in a vacuum oven at 60 ℃ for 10 h, the MnO_2 cathode was cut into discs with a diameter of 14 mm. The areal mass loading of MnO_2 was controlled at 0.8 - 1.2 mg cm^{-2}.

Preparation of coating anode. Ti_4O_7 protective layer was prepared on the surface of commercial zinc foil by a simple scraping coating method. In short, the mass fraction

of 1 % NFC was mixed with Ti_4O_7 powder to form a uniform slurry, which was coated on a 100μm commercial zinc foil with a scraper and dried at 60 °C to form a coating named Ti_4O_7@Zn. the coated zinc foil was cut into discs with a diameter of 14 mm. Cut the Ti_4O_7@Zn coating into 14 mm diameter discs for later use.

Material characterization

The crystal structure of the synthesized powders and electrode surface was characterized by X-ray diffraction (XRD, AXS D8 Advance, Bruker) with Cu Kα radiation. The surfaces of both bare Zn and Ti_4O_7@Zn electrodes before and after Zn plating were characterized by scanning electron microscopy (SEM, SU-8010F, HITACHI), the corresponding energy dispersive spectrometer (EDS) mapping was applied to analyze the element distribution. X-ray photoelectron spectroscopy analysis (XPS) was determined by a Kratos Axis Ultra spectrometer with a monochromatic Al Kα radiation (h ν = 1486.6 eV). The contact Angle of Ti_4O_7@Zn and bare Zn with electrolyte was measured by a contact Angle tester (Theta, Biolin Scientific). The in situ optical images of zinc electrodes during 2 mA cm^{-2} stripping/galvanizing were observed using a YM710R metallographic microscope (YUESCOPE, Suzhou) on zinc-zinc symmetrical cells composed of 1 cm × 1 cm zinc foils and 2 M $ZnSO_4$ electrolyte.

Computational method

We have employed the Vienna Ab Initio Package (VASP) to perform all the spin-polarized density functional theory (DFT) calculations within the generalized gradient approximation (GGA) in the PBE formulation. We have chosen the projected augmented wave (PAW) potentials to describe the ionic cores and take valence

electrons into account using a plane wave basis set with a kinetic energy cutoff of 450 eV. Partial occupancies of the Kohn−Sham orbitals were allowed using the Methfessel-Paxton smearing method and a width of 0.10 eV. The electronic energy was considered self-consistent when the energy change was smaller than 10^{-5} eV. A geometry optimization was considered convergent when the residual forces were smaller than 0.03 eV/Å. The transition state of an elementary reaction step was located by the nudged elastic band (NEB) method. In the NEB method, the path between the reactant and product was discretized into a series of images. The intermediate images were relaxed until the perpendicular forces were smaller than 0.05 eV/Å. Finally, the adsorption energies (Eads) were calculated as Eads= Ead/sub -Ead -Esub, where Ead/sub, Ead, and Esub are the total energies of the optimized adsorbate/substrate system, the adsorbate in the structure, and the clean substrate, respectively.

Electrochemical measurement

An electrochemical workstation (CHI660E, Chenhua, Shanghai, China) was used to test the Zn and Ti_4O_7@Zn electrode's Tafel plot (Tafel), Linear Sweep Voltammetry (LSV) and other components, Amperometric i-t Curve (I - t), Chronoamperometry (CA), Electrochemical impedance spectroscopy (EIS), Cyclic voltammetry (CV). Tafel curve was measured in 2 M $ZnSO_4$ electrolyte with Ti_4O_7@Zn or Zn as working electrode, platinum electrode as counter electrode, and saturated calomel electrode (SCE) as reference electrode at a scanning rate of 2 mV s^{-1} in the potential range of -0.7 − -1.3 V. For the LSV test, Ti_4O_7@Zn or Zn was used as the working electrode and counter electrode, and saturated calomel electrode as reference electrode. The scanning

rate was 1 mV s^{-1} and the potential range was -1.6 − -2.1 V in 1 M Na_2SO_4 solution. The CA test was carried out in a zinc symmetrical battery with an overpotential of -200 mV. For electrochemical impedance spectroscopy (EIS) tests, the range of applied frequency is from 0.01 to 100 kHz. And the amplitude of AC signal is 5 mV. The scanning rate of cyclic voltammogram (CV) measurement sets at 0.2 mV s^{-1}, and the range is from 0.8 to 1.8 V. The symmetric battery is composed of two same zinc electrodes and a 2 M $ZnSO_4$ electrolyte. For the full battery test, the MnO_2 electrode, a glass fiber member and the prepared zinc electrode were assembled into a coin cell. The electrolyte was 2 M $ZnSO_4$ and 0.1 M $MnSO_4$. The batteries were tested by LANHE CT3001A Battery tester (Wuhan Rand Electronics Co., LTD.), China). Constant current charge-discharge test was carried out under different current densities, and the cut-off voltage range was 0.8 ~ 1.8V.

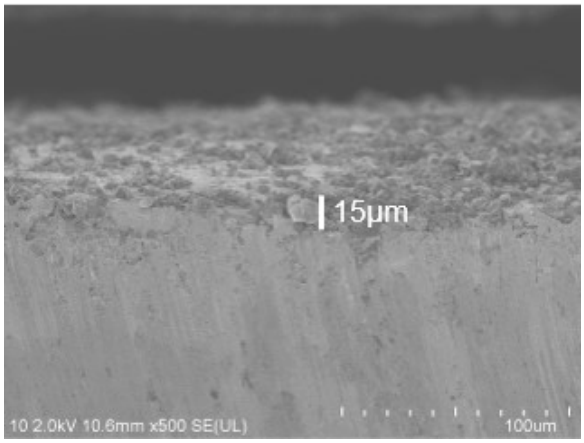

Fig. S1. SEM pattern of Ti_4O_7 coating cross section.

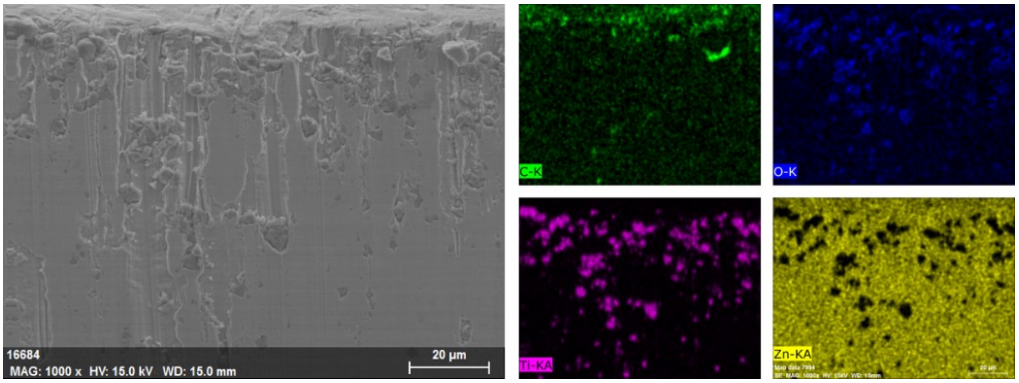

Fig. S2. EDS pattern of Ti_4O_7 coating cross section.

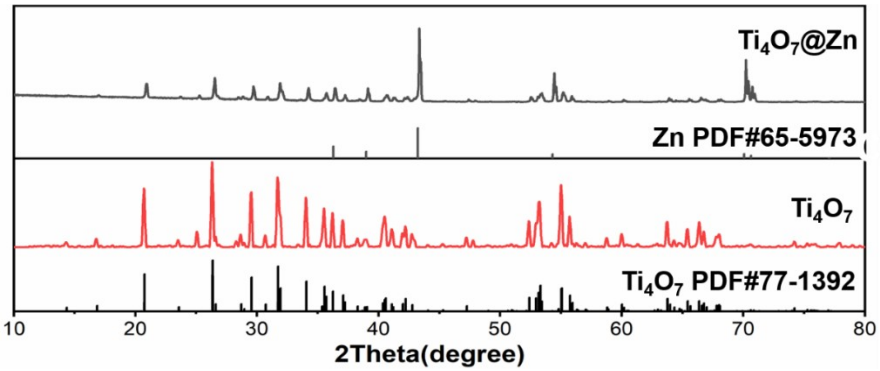

Fig. S3. XRD pattern of Ti_4O_7 powder and Ti_4O_7@Zn coating.

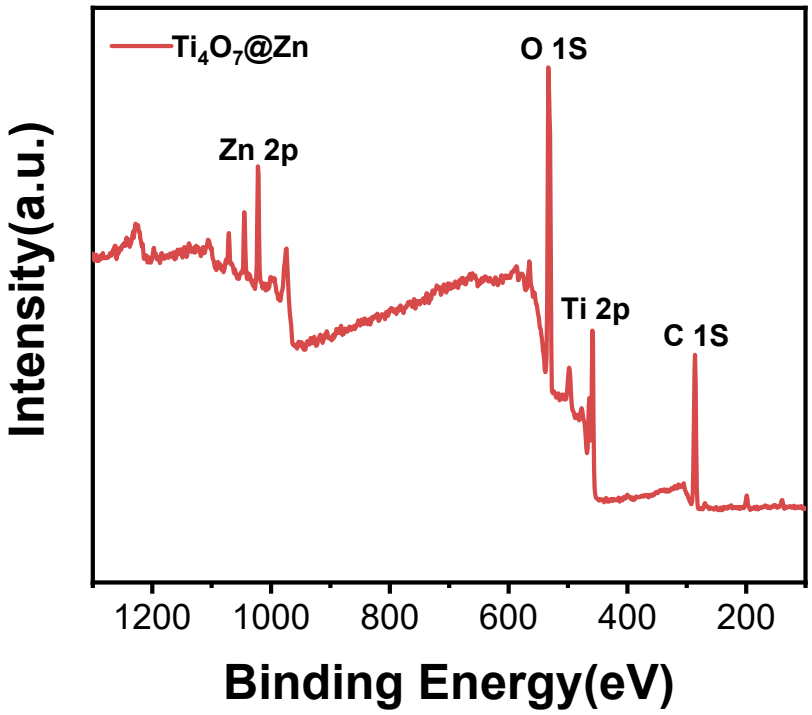

Fig. S4. XPS full spectrum of Ti_4O_7@Zn.

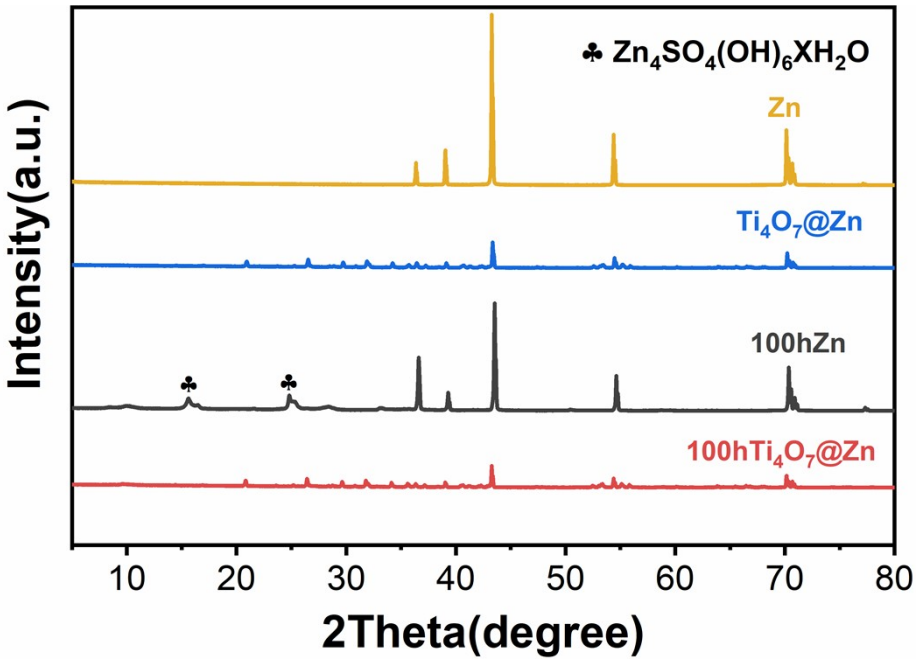

Fig. S5. XRD pattern of Zn and Ti_4O_7@Zn symmetric battery after 100 h cycle.

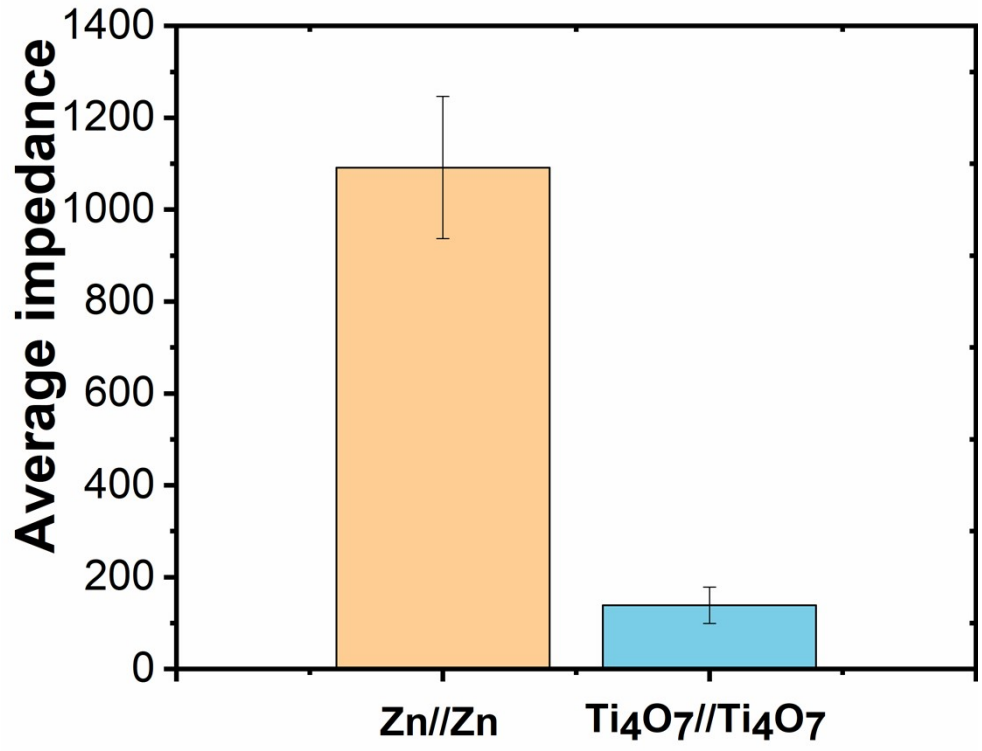

Fig. S6. Error bar diagram for Zn// Zn and Ti_4O_7// Ti_4O_7 batteries.

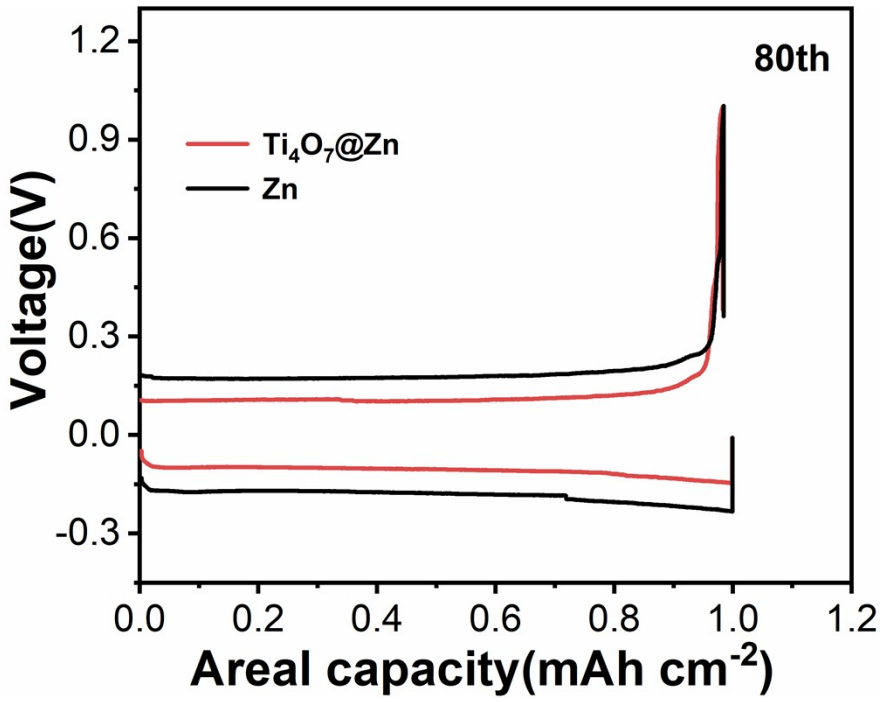

Fig. S7. Charge–discharge profiles at 80th cycle.

Fig. S8. In situ optical microscopy apparatus.

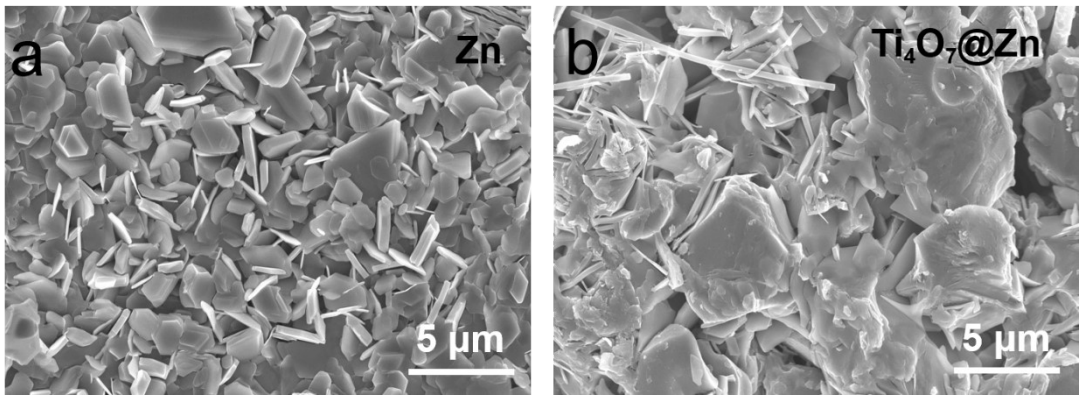

Fig. S9. SEM surface images of (a) Zn and (b) Ti_4O_7@Zn after cycling for 100 h.

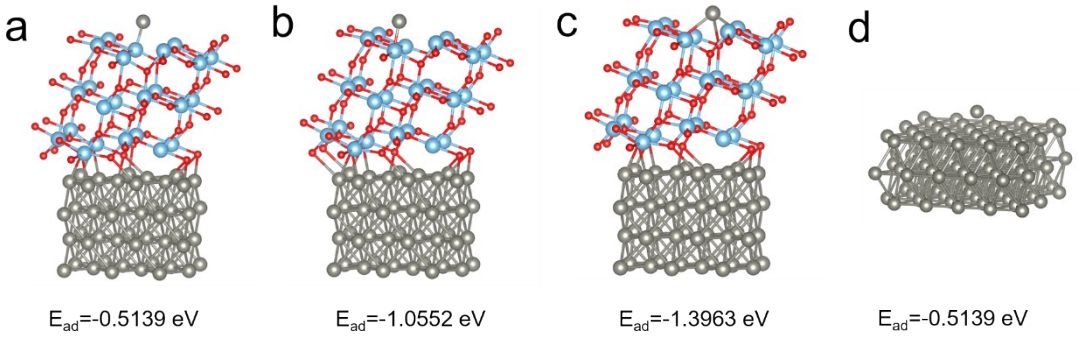

Fig. S10. Three adsorption sites and adsorption energy of Zn^{2+} on Ti_4O_7 (a) top site of Ti atom. (b) top site of O atom. (c) hollow site of Ti atom. (d) adsorption energy of Zn^{2+} on Zn surface.

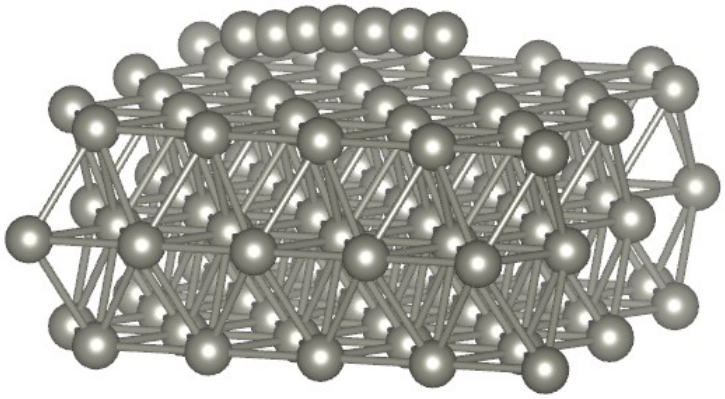

Fig. S11. Migration path of Zn^{2+} on Zn.

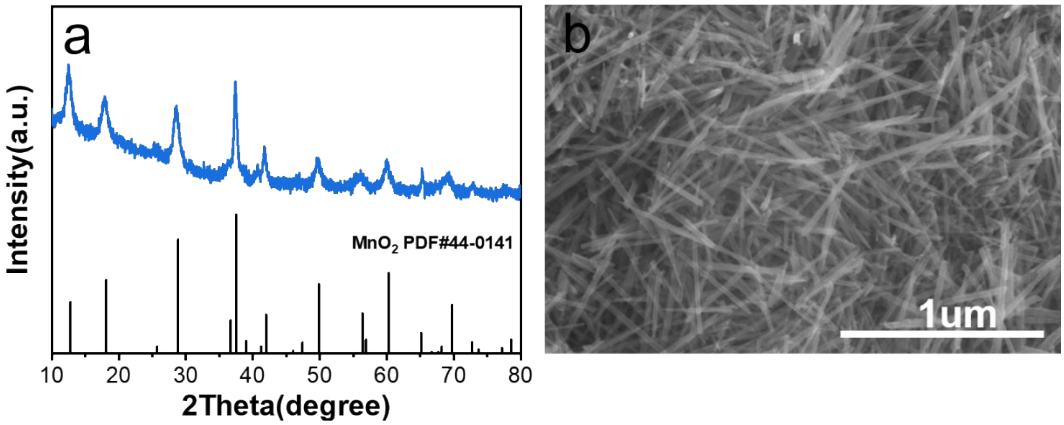

Fig. S12. (a) XRD pattern of MnO_2 (b) SEM image of MnO_2 cathode material.

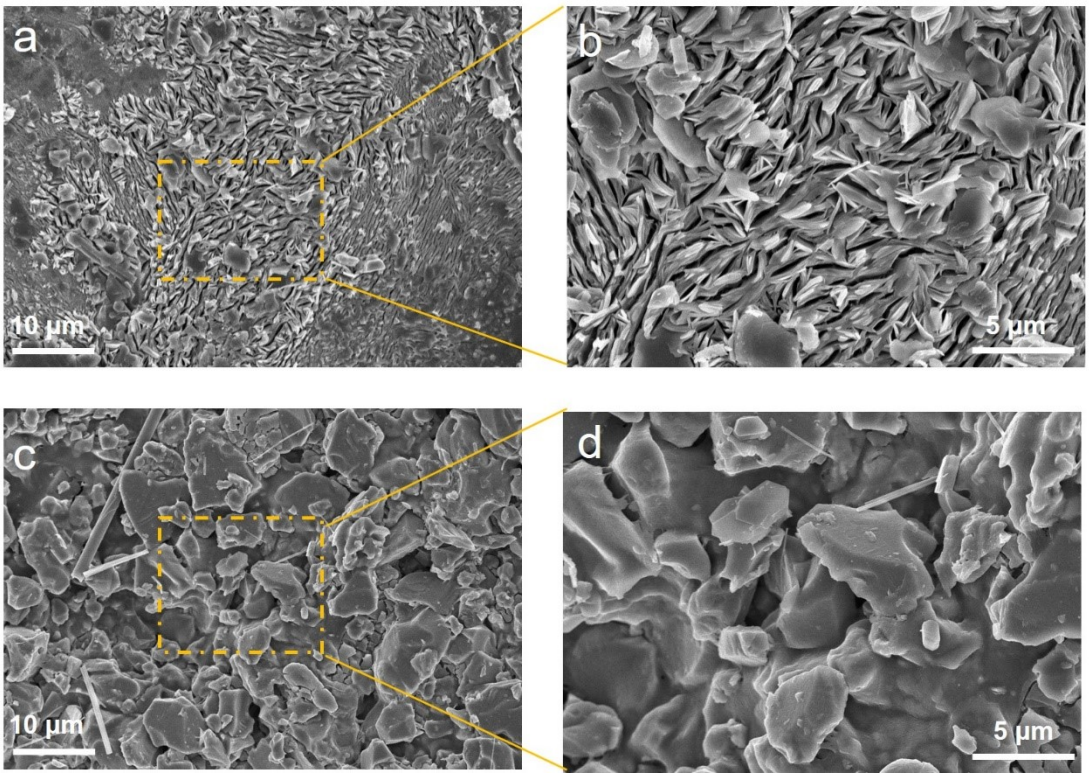

Fig. S13. SEM images of zinc anode surface of (a) bare Zn and (c) Ti_4O_7@Zn in full battery after 300 cycles at 5C; (b) is a partial enlargement of figure (a); (d) is a partial enlargement of figure (c).

Table S1. XRD refined data.

Space group:	P -1					
a	b	c	alpha	beta	gamma	occupancy
5.593056	7.119137	12.455152	95.0464	95.1845	108.7664	0.986

Zn anode	Current density/Areal capacity (mA cm^{-2}/mAh cm^{-2})	Overpotential (mV)	Lifespan (h)	Refs.
ZrO_2	1/0.5	36	1750	[1]
Zn@CrN	1/0.25	28	3700	[2]
	5/2	46	1200	
SiC@Zn	1/0.25	40	780	[3]
Zn@CaF_2	0.25/0.25	38	4000	[4]
Zn@NZP	1/0.25	44	1200	[5]
SnNc@Zn	1/1	23.8	1000	[6]
ZnSe@Zn	10/1	49	1000	[7]
TiN@Zn	1/1	30	2200	[8]
	2/2	40	1000	
Zn@HAP	1/0.25	48.4	2000	[9]
CSO-Zn	1.25/0.25	91	600	[10]
UMMT@Zn	1/0.5	40	2000	[11]
KL-Zn	4.4/1.1	70	800	[12]
Zn@ZPO	1/1	21	3500	[13]
Nb_2O_5@Zn	0.5/0.5	44	630	[14]
BTO/PVT@Zn	1/1	50	3000	[15]
Zn-ZnF_3	0.5/0.5	30	1400	[16]
$AgZn_3$@Zn	2/1	23	1360	[17]
Ti_4O_7@Zn	**1/1**	**25**	**5900**	**This**
	5/1	**52**	**3500**	**work**

Reference

[1] Y. Liu, T. Guo, Q. Liu, F. Xiong, M. Huang, Y. An, J. Wang, Q. An, C. Liu, L. Mai, Ultrathin

ZrO2 coating layer regulates Zn deposition and raises long-life performance of aqueous Zn batteries. Materials Today Energy (2022). https://doi.org/10.1016/j.mtener.2022.101056
[2] L. Gao, L. Qin, B. Wang, M. Bao, Y. Cao, X. Duan, W. Yang, X. Yang, Q. Shi, Highly-Efficient and Robust Zn Anodes Enabled by Sub-1-μm Zincophilic CrN Coatings. Small (2023). https://doi.org/10.1002/smll.202308818
[3] L. Chen-Yang, Z. Dong-Ting, C. Hao, L. Min-Peng, T. Chen-Yang, L. Mao-Cheng, Anticorrosion and Hydrophobic Surface Protection Inducing Dendrite-Free Zn Anode for Aqueous Zn-Ion Batteries. Energy Technology (2023). https://doi.org/10.1002/ente.202300885
[4] Y. Li, S. Yang, H. Du, Y. Liu, X. Wu, C. Yin, D. Wang, X. Wu, Z. He, X. Wu, A stable fluoride-based interphase for a long cycle Zn metal anode in an aqueous zinc ion battery. Journal of Materials Chemistry A 10(27) (2022) 14399-14410. https://doi.org/10.1039/d2ta03550b
[5] N. Yu, Y. Li, W. She, H. Li, H. Chen, W. Cheng, J. Chen, H. Liu, Y. Tu, Z. Huang, Y. Wan, L. Zou, X. Zhong, n. JunmingLuo, K. Guo, Binder-Free Sodium Zinc Phosphate Protection Layer Enabled Dendrite-Free Zn Metal Anode. ACS Applied Materials & Interfaces (2022). https://doi.org/10.1021/acsami.2c13499
[6] W. Yijie, T. Yan, C. Chuanwei, Atomic Sn sites on nitrogen-doped carbon as a zincophilic and hydrophobic protection layer for stable Zn anodes. Journal of Materials Chemistry A (2023). https://doi.org/10.1039/d3ta06372k
[7] Q. Li, H. Hong, J. Zhu, Z. Wu, C. Li, D. Wang, P. Li, Y. Zhao, Y. Hou, G. Liang, F. Mo, H. Cui, C. Zhi, Crystal Orientation Engineering of Perfectly Matched Heterogeneous Textured ZnSe for an Enhanced Interfacial Kinetic Zn Anode. ACS Nano (2023). https://doi.org/10.1021/acsnano.3c07848
[8] J. Zheng, Z. Cao, F. Ming, H. Liang, Z. Qi, W. Liu, C. Xia, C. Chen, L. Cavallo, Z. Wang, H.N. Alshareef, Preferred Orientation of TiN Coatings Enables Stable Zinc Anodes. ACS Energy Letters 7(1) (2021) 197-203. https://doi.org/10.1021/acsenergylett.1c02299
[9] Q. Han, L. Cai, P. Huang, S. Liu, C. He, Z. Xu, H. Ying, W.-Q. Han, Fast Ionic Conducting Hydroxyapatite Solid Electrolyte Interphase Enables Ultra-Stable Zinc Metal Anodes. ACS Applied Materials & Interfaces (2023). https://doi.org/10.1021/acsami.3c11649
[10] P. Zhai, X. Zhai, Z. Jia, W. Zhang, K. Pan, Y. Liu, Inhibiting corrosion and side reactions of zinc metal anode by nano-CaSiO3 coating towards high-performance aqueous zinc-ion batteries. Nanotechnology (2022). https://doi.org/10.1088/1361-6528/aca1cd
[11] M. Liu, A. Hu, Z. Yan, J. Chen, M. He, B. Zhou, Y. Pan, Y. Fan, D. Gao, J. Long, Enhancing Zn2+ diffusion for dendrite-free zinc anodes via a robust zincophilic clay mineral coating. Chemical Engineering Journal (2023). https://doi.org/10.1016/j.cej.2023.147410
[12] C. Deng, X. Xie, J. Han, Y. Tang, J. Gao, C. Liu, X. Shi, J. Zhou, S. Liang, A Sieve-Functional and Uniform-Porous Kaolin Layer toward Stable Zinc Metal Anode. Advanced Functional Materials 30(21) (2020). https://doi.org/10.1002/adfm.202000599
[13] X. Song, L. Bai, C. Wang, D. Wang, K. Xu, J. Dong, Y. Li, Q. Shen, J. Yang, Synergistic Cooperation of Zn(002) Texture and Amorphous Zinc Phosphate for Dendrite-Free Zn Anodes. ACS Nano (2023). https://doi.org/10.1021/acsnano.3c04343
[14] X. Li, P. Ye, A. Dou, Z. Jiang, A. Naveed, Y. Zhou, M. Su, P. Zhang, Y. Liu, Nanoporous Nb2O5 coatings enabled long-life and deeply rechargeable zinc anodes for aqueous zinc-ion batteries. Journal of Energy Storage 76 (2024). https://doi.org/10.1016/j.est.2023.109874
[15] Z. Quan, L. Bo, L. Chaofeng, Y. Yifei, K. Qiaoling, L. Dongyun, Z. Zejie, T. Daiwen, Z. Jingji, W. Jiangying, Z. Qilong, C. Guozhong, Dendrite-Free and Highly Stable Zn Metal Anode with

BaTiO3/P(VDF-TrFE) Coating. ACS Energy Letters (2023). https://doi.org/10.1021/acsenergylett.3c01017
[16] Y. Zhou, H. Tong, Y. Wu, X. Chen, C. Wu, Z. Xu, L. Shen, X. Zhang, A Dendrite-Free Zn Anode Co-modified with In and ZnF(2) for Long-Life Zn-Ion Capacitors. ACS Appl Mater Interfaces 14(41) (2022) 46665-46672. https://doi.org/10.1021/acsami.2c13536
[17] H. Lu, Q. Jin, X. Jiang, Z.M. Dang, D. Zhang, Y. Jin, Vertical Crystal Plane Matching between AgZn(3) (002) and Zn (002) Achieving a Dendrite-Free Zinc Anode. Small 18(16) (2022) e2200131. https://doi.org/10.1002/smll.202200131